

Focusing on Warm Dark Matter with Lensed High-redshift Galaxies

Fabio Pacucci¹ *, Andrei Mesinger¹, Zoltán Haiman²

¹*Scuola Normale Superiore, Piazza dei Cavalieri, 7 56126 Pisa, Italy*

²*Department of Astronomy, Columbia University, 550 West 120th Street, New York, NY, 10027, U.S.A.*

submitted to MNRAS

ABSTRACT

We propose a novel use of high-redshift galaxies, discovered in deep Hubble Space Telescope (HST) fields around strong lensing clusters. These fields probe small comoving volumes ($\sim 10^3$ Mpc³) at high magnification ($\mu \gtrsim 10$), and can detect otherwise inaccessible ultra-faint galaxies. Even a few galaxies found in such small volumes require a very high number density of collapsed dark matter (DM) halos. This implies significant primordial power on small scales, allowing these observations to rule out popular alternatives to standard cold dark matter (CDM) models, such as warm dark matter (WDM). In this work, we analytically compute WDM halo mass functions at $z = 10$, including the effects of both particle free-streaming and residual velocity dispersion. We show that the two $z \approx 10$ galaxies already detected by the Cluster Lensing And Supernova survey with Hubble (CLASH) survey are sufficient to constrain the WDM particle mass to $m_x > 1$ (0.9) keV at 68% (95%) confidence limit (for a thermal relic relativistic at decoupling). This limit depends only on the WDM halo mass function and, unlike previous constraints on m_x , is independent of any astrophysical modeling. The forthcoming HST Frontier Fields can significantly tighten these constraints.

Key words: cosmology: theory - early universe - dark matter - galaxies: large-scale structure of universe - high-redshift

1 INTRODUCTION

The Λ CDM cosmological model, in which structure formation proceeds in a hierarchical manner driven by pressure-less cold dark matter (CDM), has been remarkably successful in predicting the matter distribution on large scales. It accurately describes the statistical properties of the cosmic microwave background (CMB), cluster abundances, galaxy clustering and the cosmic web (e.g. Tegmark et al. 2006; Benson 2010; Komatsu et al. 2011; Hinshaw et al. 2012).

However, observations of low-redshift galaxies over the past decade have suggested that CDM predicts too much power on small scales. For instance, CDM N -body simulations contain more satellite galaxies than are observed both around our galaxy (the so-called “missing satellite problem”), in voids, and in the field (e.g. Moore et al. 1999; Klypin et al. 1999; Diemand et al. 2008; Springel et al. 2008; Papastergis et al. 2011; Ferrero et al. 2012). The inner profiles of individual dwarf galaxies are too shallow, compared with CDM predictions (e.g. Moore et al. 1994; de Blok et al. 2001; Macciò et al. 2012; Governato et al. 2012). Furthermore, CDM simulations result in a population of massive, concentrated Galactic sub-halos that are inconsistent with kinematic observations of the bright Milky Way satellites (Boylan-Kolchin et al. 2012).

An apparent solution can be found by appealing to the

baryons. Baryonic feedback caused by supernovae explosions and heating due to the UV background may suppress the baryonic content of low-mass halos and make their inner density profile shallower (e.g. Governato et al. 2007; Mashchenko et al. 2008; Busha et al. 2010; Sobacchi & Mesinger 2013; Teyssier et al. 2013). Nevertheless, it is not clear if baryonic feedback provides a satisfactory match to all observations, even when its implementation is “tuned” relatively arbitrarily (e.g. Boylan-Kolchin et al. 2012; Garrison-Kimmel et al. 2013; Teyssier et al. 2013).

An alternative explanation might be found if dark matter consisted of lower mass¹ (\sim keV) particles, so-called warm dark matter (WDM; Blumenthal et al. 1982). Given their lower mass with respect to cold dark matter, WDM particles remain relativistic for a longer time and they are able to free-stream out of potential wells, smearing out small-scale primordial perturbations. In addition, their velocity dispersion acts as an effective pressure which suppresses growth of perturbations on scales smaller than a characteristic Jeans mass. Therefore, small-scale structure is dramatically suppressed in WDM models, and models with WDM masses of $m_x \sim$ keV might provide a better match to observations of lo-

¹ Throughout this work, we report warm dark matter particle masses, m_x , assuming thermal relics which were relativistic at decoupling (e.g. neutralino, gravitino). Results can be translated for non-thermal relics, such as the sterile neutrino, by equating their free-streaming lengths, though care should be taken in interpreting the effects of residual velocities in those cases (see below).

* fabio.pacucci@sns.it

cal galaxies (e.g. Bode et al. 2001; Khlopov & Kouvaris 2008; Valageas 2012; Kang et al. 2013; Angulo et al. 2013; Viel et al. 2013; though see Macciò et al. 2012 and Shao et al. 2013 who argue that the required WDM masses are low enough to be ruled out by current observations).

The most powerful test-bed for these scenarios is the high-redshift Universe. Structure formation in WDM models (or in any cosmological model with an equivalent power-spectrum cut-off) is exponentially suppressed on small scales. Since in a CDM dominated Universe structures form hierarchically, these small halos are expected to host the first galaxies². Therefore, the mere presence of a galaxy at high-redshift ($z \gtrsim 10$) can set strong lower limits on the WDM particle mass (e.g. Barkana et al. 2001; Mesinger et al. 2005).

Various high- z observations have already been used to constrain WDM properties. WDM masses lower than $m_x \approx 3$ keV would smear out the Lyman alpha forest seen in high- z quasar spectra (Viel et al. 2008; Viel et al., in preparation). Somewhat weaker limits, $m_x \gtrsim 0.75$ keV are obtained by simultaneously reproducing the stellar mass function and the Tully-Fisher relation (Kang et al. 2013). Requiring that reionization is completed by $z \gtrsim 6$ yields a similar limit, as does the need to grow $\sim 10^9 M_\odot$ super-massive black holes by this redshift (Barkana et al. 2001). However, most of these limits are strongly affected by a degeneracy between astrophysical processes (involving baryons) and the dark matter mass. Recently, de Souza et al. (2013) set robust limits of $m_x > 1.6 - 1.8$ keV (95% confidence level) from the number of high- z gamma ray bursts (GRBs) observed with *Swift*, using a Bayesian likelihood analysis as well as conservative assumptions to minimize degeneracy with the astrophysics.

In this work we show how the abundances of lensed, very high-redshift galaxies can be used to robustly probe primordial small-scale power, as typified by WDM models. Lensing facilitates the detection of ultra-faint high- z galaxies in fairly small volumes. The mere detection of a single halo in this volume would imply a very high number density, setting a tight upper limit on the WDM particle mass, *completely independent of astrophysical degeneracies*. Currently, there are two highly magnified galaxy candidates at $z \sim 10$, discovered as part of the Cluster Lensing And Supernova survey with Hubble (CLASH; Postman et al. 2012; Zheng et al. 2012; Coe et al. 2013). MACS1149-JD is at $z = 9.6 \pm 0.2$, magnified by a factor of $\mu \sim 15$. MACS0647-JD at $z = 10.7^{+0.6}_{-0.4}$ has three images, one of which is magnified by a factor of $\mu \sim 8$.

The outline of this paper is as follows. In §2 we discuss how we derive dark matter halo mass functions in both CDM and WDM models. In §3 we present the resulting mass functions at $z = 10$, comparing them with recent CLASH observations. In §4 we discuss future improvements, while in §5 we report our conclusions. Throughout, we adopt recent Planck cosmological parameters: $(\Omega_m, \Omega_\Lambda, \Omega_b, h, n_s, \sigma_8) = (0.32, 0.68, 0.05, 0.67, 0.96, 0.83)$, and assume WDM is a fermionic spin 1/2 particle. All scales are quoted in comoving units, unless otherwise indicated.

² Once larger scales go nonlinear at lower redshifts, in principle, low-mass halos can form in WDM models via top-down fragmentation, spoiling such direct inferences (e.g. Bode et al. 2001; however, such fragmentation is exceedingly difficult to simulate reliably, see Wang & White 2007). At sufficiently high redshifts, before *any* scales go nonlinear, no halos of any mass exist.

2 MASS FUNCTIONS IN CDM AND WDM

In WDM models the growth of density perturbations is suppressed on small scales. This is due to a combination of two different effects: (i) particle free-streaming during the radiation-dominated era smears-out small-scale structure, altering the effective transfer function of the matter power spectrum (e.g. Bode et al. 2001); and (ii) the stochastic residual velocity dispersion of particles, although redshifting away as $\propto (1+z)$, suppresses the initial growth of DM perturbations, acting as an effective pressure term. Below, we describe how we account for these two effects in constructing analytic mass functions, closely following the procedure recently outlined in Benson et al. (2013).

2.1 Power spectrum cut-off from WDM free-streaming

The free-streaming scale for a thermal relic, defined as the scale at which the linear perturbation amplitude is suppressed by a factor of two, is given by (Bode et al. 2001)

$$R_{\text{fs}} \approx 0.31 \left(\frac{\Omega_x}{0.3} \right)^{0.15} \left(\frac{h}{0.65} \right)^{1.3} \left(\frac{\text{keV}}{m_x} \right)^{1.15} \frac{\text{Mpc}}{h}, \quad (1)$$

where Ω_x is the fraction of the critical energy density contained in WDM, and h is the Hubble constant in units of $100 \text{ km s}^{-1} \text{ Mpc}^{-1}$. The free-streaming scale corresponding to $m_x = 1$ keV is $R_{\text{fs}} \approx 0.52$ Mpc. The corresponding modification of the matter power spectrum can be computed by multiplying the CDM power spectrum $P_{\text{CDM}}(k)$ by an additional scale-dependent transfer function (Bode et al. 2001):

$$P_{\text{WDM}}(k) = P_{\text{CDM}}(k) [1 + (\epsilon k)^{2\mu}]^{-5\mu}, \quad (2)$$

where $\mu = 1.12$ and

$$\epsilon = 0.049 \left(\frac{\Omega_x}{0.25} \right)^{0.11} \left(\frac{m_x}{\text{keV}} \right)^{-1.11} \left(\frac{h}{0.7} \right)^{1.22} h^{-1} \text{Mpc}. \quad (3)$$

The root variance in the $z = 0$ linearly-interpolated matter field on scale M is then computed according to:

$$\sigma^2(M) = \frac{1}{2\pi^2} \int_0^\infty 4\pi k^2 P(k) W^2(k|M) dk \quad (4)$$

We use a sharp k-space filter window function in the case of WDM,

$$W(k|M) = \begin{cases} 1 & \text{if } k \leq k_s(M) \\ 0 & \text{if } k > k_s(M) \end{cases} \quad (5)$$

relating the cut-off mode k_s to the spatial scale $R = [3M/(4\pi\bar{\rho})]^{1/3}$ through $k_s = 2.5/R$. Benson et al. (2013) show that this choice of window function and normalization accurately reproduces WDM mass functions from N -body simulations.

2.2 Effective pressure from WDM residual velocities

Structure formation in WDM models will be further suppressed by the residual velocity dispersion of the WDM particles, which delays the growth of perturbations. This effect can be incorporated in the halo mass function by raising the critical overdensity threshold required for collapse, $\delta_c(M, z)$. Using spherically symmetric hydrodynamics simulations, and exploiting the analogy between the WDM effective pressure and gas pressure, Barkana et al. (2001) computed the modified $\delta_c(M, z)$ to be used in the excursion-set random walk procedure. They show that this effective pressure can be of comparable importance to the power spectrum cut-off above,

in suppressing small-scale structures. Benson et al. (2013) showed that the results of Barkana et al. (2001) can be well fitted by the following functional form:

$$\delta_{c,\text{WDM}}(M, z) = \delta_{c,\text{CDM}}(t) \left\{ h(x) \frac{0.04}{\exp(2.3x)} + \right. \quad (6)$$

$$\left. + [1 - h(x)] \exp \left[\frac{0.31687}{\exp(0.809x)} \right] \right\}. \quad (7)$$

Here $x = \log(M/M_J)$ and M_J is an effective WDM Jeans mass, i.e., the mass scale below which collapse is significantly delayed by the pressure:

$$M_{\text{WDM}} \sim 3.06 \times 10^8 \left(\frac{\Omega_x h^2}{0.15} \right)^{1/2} \left(\frac{m_x}{\text{keV}} \right)^{-4} \times \quad (8)$$

$$\times \left(\frac{1 + z_{\text{eq}}}{3000} \right)^{1.5} \left(\frac{g_x}{1.5} \right)^{-1} M_{\odot}, \quad (9)$$

where z_{eq} is the redshift of radiation-matter equality, g_x is the effective number of degrees of freedom of WDM, and

$$h(x) = \left\{ 1 + \exp \left[\frac{x + 2.4}{0.1} \right] \right\}^{-1}. \quad (10)$$

Benson et al. (2013) also note that $\delta_{c,\text{WDM}}(M, z)$ should be multiplied by an additional factor of 1.197, in order to compensate for the non-standard normalization of the window function above. This normalization is motivated by requiring WDM and CDM mass functions to converge at high masses. In order to compute the WDM mass function, one can record the first crossing probability, $f(\sigma^2)$, averaging over many random walks (Barkana et al. 2001; Mesinger et al. 2005). Instead we use the faster recursive procedure described in Appendix A of Benson et al. (2013), to which we refer the reader for further details.

2.3 CDM mass functions

We adopt a standard analytic formula, which is known to accurately fit N -body results (Sheth & Tormen 1999; Jenkins et al. 2001), to compute CDM mass functions:

$$f_{\text{ST}} = A \sqrt{\frac{2a_1}{\pi}} \times \left[1 + \left(\frac{\sigma^2}{a_1 \delta_c^2} \right)^p \right] \times \frac{\delta_c}{\sigma} \exp \left(-\frac{a_1 \delta_c^2}{2\sigma^2} \right) \quad (11)$$

where f_{ST} is the fraction of mass contained in halos with masses greater than M , and $A = 0.322$, $a_1 = 0.707$, $p = 0.3$, $\delta_c = 1.686$. The mass fractions, f_{ST} , can be related to the halo number density $n_{\text{ST}}(M, z)$ through

$$f_{\text{ST}} = \frac{M}{\rho_m} \frac{dn_{\text{ST}}(M, z)}{d \ln \sigma^{-1}} \quad (12)$$

where ρ_m is the total mass density of the background Universe.

3 RESULTS

The resulting CDM and WDM halo mass functions at $z = 10$ are shown in Figure 1, for four different values of the WDM particle mass: $m_x = 0.5, 1.0, 1.5, 2.0$ keV. Solid lines include both of the effects mentioned above (free-streaming and effective pressure), while dashed lines only include the free-streaming. The latter can be considered as strict, highly-conservative, particle-type independent estimates of the impact of WDM on high- z mass functions³.

³ The effects of free-streaming (§2.1) are straightforward to compute analytically and to include in N -body simulations as a modification of the

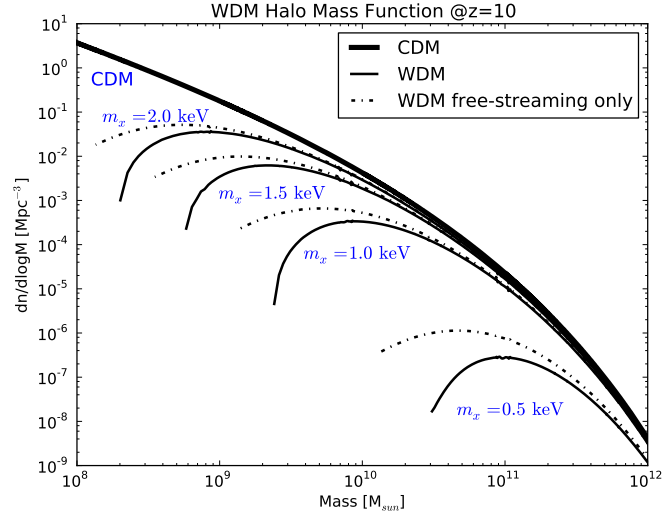


Figure 1. Halo mass functions in CDM (thick solid line) and WDM (solid lines) at $z = 10$. The dot-dashed lines correspond to WDM models where only the free-streaming effect has been accounted for (i.e. the effective pressure from the residual velocity dispersion of the WDM particles is neglected).

The thick solid line is the standard CDM halo mass function. The exponential suppression of low-mass halos in WDM models is evident in the figure, with the abundance of $\sim 10^8 M_{\odot}$ halos dramatically reduced for $m_x \lesssim 2$ keV. The effective pressure from WDM velocity dispersion makes this mass function truncation much more dramatic (c.f. Barkana et al. 2001; Mesinger et al. 2005). Halos with $M \approx 10^8 M_{\odot}$ correspond to the lowest masses in which cooling by atomic hydrogen is efficient, suggesting that abundances of $z \sim 10$ star-forming galaxies are sensitive to $m_x \lesssim 2-3$ keV (e.g., de Souza et al. 2013).

By integrating the WDM mass functions in Figure 1 above a low-mass limit, M_{min} , one obtains the total number density of halos at $z = 10$ with mass $M > M_{\text{min}}$, shown in Figure 2. This figure is the main result of this work. As an example of its use, let us consider halo abundances in WDM models with $m_x < 3$ keV. We note from the figure that halos, of any mass, cannot be more abundant than $\approx 0.8 \text{ Mpc}^{-3}$ if $m_x \lesssim 3$ keV. This “forbidden region” is highlighted in blue, and is completely independent of the physics of the baryons. In principle, stronger constraints could be obtained, at the expense of astrophysical modeling uncertainties, if such modeling requires host halos of detected galaxies to be higher than $M_{\text{min}} \gtrsim 10^9-10^{10} M_{\odot}$. For example, considering that

initial power spectrum (e.g. Bode et al. 2001). Analytic WDM halo mass functions are in agreement with N -body codes, when compared just including free-streaming and accounting for artificial fragmentation of N -body filaments (Wang & White 2007). Furthermore, the resulting modification of the power spectrum can be computed for any given WDM particle, and so results for our fiducial thermal relic mass, m_x , can be translated to masses of other WDM particles (e.g. sterile neutrinos), by equating their corresponding streaming lengths. On the other hand, the effects of WDM velocity dispersion (§2.2) are more uncertain, as they require accounting for intra-particle dispersion in N -body simulations. Thus our prescription for including the effects of residual velocities on structure formation is not as well tested as the effects of free-streaming. Furthermore, our method is motivated by the results of Barkana et al. (2001), who made the analogy of WDM velocity dispersion to gas temperature in their simulations. This analogy is only well defined in the case of a thermal relic WDM particle.

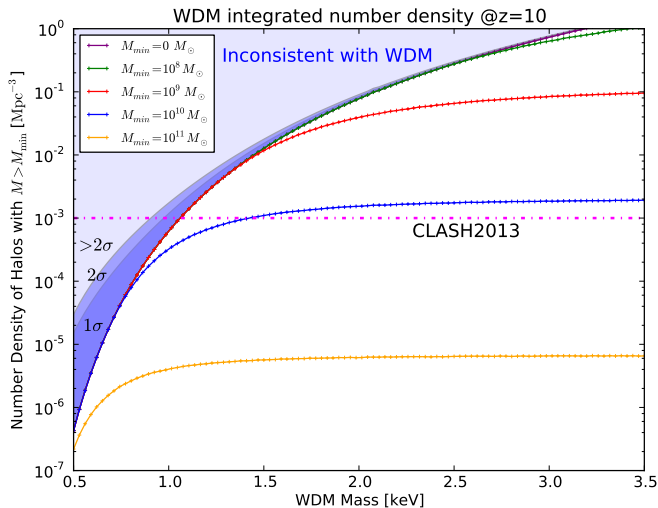


Figure 2. Integrated number densities of WDM halos as a function of the particle mass, m_x . Abundances were computed down to a minimum halo mass, M_{\min} . The shaded region corresponds to abundances higher than those integrating all the way down to $M_{\min} = 0 M_{\odot}$ (i.e. with no lower limit on the halo mass), and are strictly ruled out. The number density implied by the two lensed CLASH candidates is demarcated with a horizontal purple line. The darker shaded regions corresponds to the 1 and 2 sigma Poisson uncertainties on the number predicted by the $M_{\min} = 0 M_{\odot}$ models for the CLASH volume cited in the text. The striking difference between the 1 sigma and 2 sigma levels is due to the log-scale used.

star-forming galaxies at this redshift⁴ are unlikely to be hosted by halos less massive than the corresponding atomic cooling threshold (i.e. with virial temperatures less than $\approx 10^4$ K, corresponding to $M_{\min} \approx 10^8 M_{\odot}$ at $z = 10$), one can set only a modestly stronger⁵ upper limit on the *abundance of star-forming galaxies* corresponding to the green curve, $\lesssim 0.6 \text{ Mpc}^{-3}$ for $m_x \lesssim 3 \text{ keV}$. Further including some modeling of the halo mass \rightarrow galaxy luminosity, combined with the telescope sensitivity limits, allows one to obtain estimates of the *abundances of observable galaxies*⁶.

We now consider the current limits available from the two CLASH lensing candidates. The total effective volume, $V_{\text{eff}}(\mu)$, is a function of the magnification factor, μ , with higher magnification factors corresponding to smaller effective volumes. Currently the first 12 clusters (out of a total of 25) have been processed, with $V_{\text{eff}}(\mu)$ computed. The two lensing candidates from CLASH, along with the 12-cluster comoving volume at that magnification, $V_{\text{eff}}(\mu)$, are listed in the table below (Moustakas, L. A., private communication):

⁴ The very first galaxies are expected to be hosted by less massive halos, in which gas cooled via the molecular cooling channel. However, the H_2 -disassociating background likely sterilized star formation in these galaxies long before $z = 10$ (e.g., Haiman & Loeb 1997; McQuinn & O’Leary 2012).

⁵ Since our WDM mass functions truncate abruptly towards low masses, there are virtually no halos with masses lower than $\lesssim 10^8 M_{\odot}$, even for particle masses as high as $m_x \sim 3 \text{ keV}$.

⁶ Note that the observed Lyman break galaxy candidates at $z \sim 6-8$ are expected to be hosted by $M_{\min} \gtrsim 10^{10} - 10^{11} M_{\odot}$ halos, when abundances are computed within a CDM framework, and these relatively large halo masses are generally consistent with the observed Lyman α fluxes (e.g. Bouwens et al. 2008; Labbe et al. 2010).

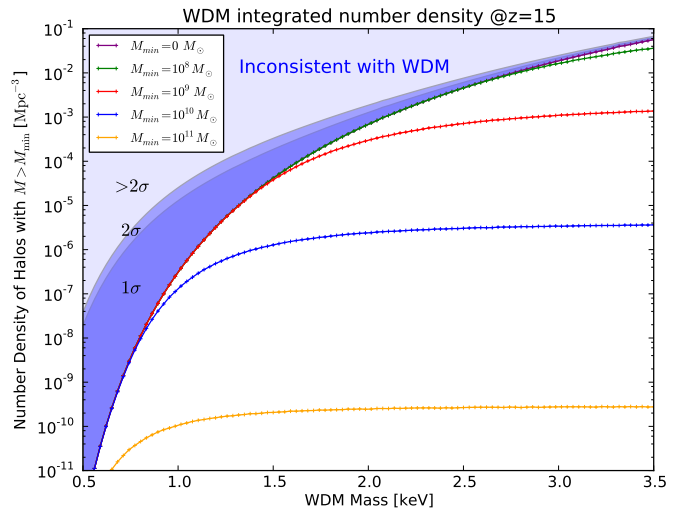


Figure 3. Same as Fig. 2, but computed at $z = 15$.

Object ID	μ	$V_{\text{eff}}(\mu) [\text{Mpc}^3]$
MACS1149-JD	15	~ 700
MACS0647-JD	8	~ 2000

The effective volumes are very small, and hence the implied abundances relatively large. If we conservatively take the volume corresponding to the lower magnification, the two candidates give a number density of $2/2000 \text{ Mpc}^{-3}$, or:

$$n_{\text{tot}} \sim 10^{-3} \text{ Mpc}^{-3}. \quad (13)$$

This total number density is shown by the dashed horizontal purple line in Figure 2.

The intersection of this horizontal line with the edge of the “forbidden region” provides the robust constraint of $m_x > 1 \text{ keV}$. For this constraint, we have included the 1- σ Poisson errors (68% confidence limit; C.L.) on the expectation value for the number of predicted halos in the total CLASH volume in the $M_{\min} = 0$ models (shown as the dark blue shaded region in Fig. 2). The corresponding 2- σ constraint (95% C.L.) is $m_x > 0.9 \text{ keV}$ (medium blue shaded region). This constraint is competitive with other current WDM constraints discussed above. More importantly however, *it is the only constraint on the WDM particle mass completely independent of astrophysics.*

For reference, we have also computed the WDM halo number densities ignoring the effects of peculiar velocities. We find that ignoring the effects of peculiar velocities (i.e. only accounting for free-streaming) mildly degrades the above constraints from CLASH, to $m_x > 0.9 \text{ keV}$ (68% C.L.).

Estimates of the halo number densities at higher redshifts could provide even tighter constraints on the WDM particle mass. For example, if an object at $z \sim 15$ was discovered in a similar volume, the WDM constraint would strengthen to $m_x > 2.2 \text{ keV}$ (see Fig. 3). Or looking at it from a different perspective, for a $m_x = 1 \text{ keV}$ model, one would need to cover a comoving volume which is 10^5 times larger than that of CLASH, in order to find a single object at $z \sim 15$.

We note also that MACS0647-JD has multiple images, and can therefore confidently be considered to be a real $z \sim 10$ galaxy. Using the number density implied by just this one galaxy, $n_{\text{tot}} \sim 5 \times 10^{-4} \text{ Mpc}^{-3}$, our constraints would degrade to $m_x > 0.8 \text{ keV}$.

4 FUTURE POTENTIAL

Our framework can be used with future datasets. Presently the CLASH survey has full data on 23 out of a total 25 lensing clusters, with analysis completed on 12 out of the full 25 (Moustakas, L. A., private communication). Our results can be updated when the final CLASH number density becomes known. Future, deeper cluster surveys can also improve on the observed number density by detecting even fainter galaxies, closer to the WDM cut-off. In particular, the HST Frontier Fields⁷ will target 4-6 lensing clusters, and obtain images ≈ 3 magnitudes deeper than CLASH, probing an order of magnitude fainter galaxies, residing in lower-mass halos.

For a more robust constraint, the full lensing geometry of each cluster can be modeled, accounting for both the error bars on the modeled $V_{\text{eff}}(\mu)$, the redshift evolution of the mass function across this volume (since the lensed volume is not a simple comoving cube around $z = 10$), as well as the correlation function of the halos (as the sampling statistics are not quite Poisson, due to the clustering of halos). We defer these to future work.

Tighter constraints on m_x can also be obtained at the cost of including astrophysical uncertainties. Our constraints above are based on the presence of *any halos* (i.e. using $M_{\text{min}} = 0 M_{\odot}$). As mentioned above, if we consider that luminous galaxies must be hosted by relatively large halos, our constraints can improve. Relating the galaxy luminosity to the host halo mass is very uncertain, though one can make conservative choices for M_{min} . This is because, as shown in Fig. 1, the peak halo mass in WDM models can be significantly below $10^{10} M_{\odot}$ - if sufficiently luminous objects are found, their corresponding host halo masses implied by abundance matching would require uncomfortably low mass-to-light ratios in WDM models. In the extreme limit, the mass-to-light ratio could be lower than obtained by even allowing all of the baryons to form stars in a single burst. Likewise, if the observed color of a lensed galaxies implies an age older than $\gtrsim 100$ Myr, this would imply the existence of DM halos at $z \gtrsim 12$, again strengthening constraints. Nevertheless, pushing limits beyond $m_x \gtrsim 2-3$ keV would require going to even higher redshifts, since at those particle masses even the $M_{\text{min}} \approx 10^8-10^9 M_{\odot}$ abundances asymptote to CDM values (see also Fig. 1 in de Souza et al. 2013).

5 CONCLUSIONS

Structure formation in WDM models (or any similar model with a steep power-spectrum cut-off) is dramatically suppressed at small-scales. Low-mass halos can only form via top-down fragmentation at late times. This leads to a dramatic difference between halo abundances in CDM and WDM models at the high redshifts, with the Universe becoming increasingly empty as the WDM particle mass, m_x , is decreased.

In this work, we illustrate how the high implied abundances of lensed galaxies at $z \sim 10$ can be used to set robust constraints on m_x . Using two $z \sim 10$ galaxies observed to date by CLASH, we set lower limits of $m_x > 1$ (0.9) keV at 68% (95%) C.L.. This limit is the first constraint on m_x strictly independent of any astrophysical degeneracies – the only modeling required is that of the DM halo mass function (which should be verified in future numerical WDM simulations, targeting $z \gtrsim 10$) and of the effective volume of the lensing observations.

We thank Leonidas A. Moustakas and other members of the CLASH survey team for providing current estimates of the effective lensed survey volume. This was supported by the NSF under grant AST-1210877.

REFERENCES

- Angulo R. E., Hahn O., Abel T., 2013, ArXiv e-prints
 Barkana R., Haiman Z., Ostriker J. P., 2001, ApJ, 558, 482
 Benson A. J., 2010, Physics Reports, 495, 33
 Benson A. J., et al., 2013, MNRAS, 428, 1774
 Blumenthal G. R., Pagels H., Primack J. R., 1982, Nature, 299, 37
 Bode P., Ostriker J. P., Turok N., 2001, ApJ, 556, 93
 Bouwens R. J., Illingworth G. D., Franx M., Ford H., 2008, ApJ, 686, 230
 Boylan-Kolchin M., Bullock J. S., Kaplinghat M., 2012, MNRAS, 422, 1203
 Busha M. T., Alvarez M. A., Wechsler R. H., Abel T., Strigari L. E., 2010, ApJ, 710, 408
 Coe D., et al., 2013, ApJ, 762, 32
 de Blok W. J. G., McGaugh S. S., Bosma A., Rubin V. C., 2001, ApJ, 552, L23
 de Souza R. S., Mesinger A., Ferrara A., Haiman Z., Perna R., Yoshida N., 2013, ArXiv e-prints
 Diemand J., Kuhlen M., Madau P., Zemp M., Moore B., Potter D., Stadel J., 2008, Nature, 454, 735
 Ferrero I., Abadi M. G., Navarro J. F., Sales L. V., Gurovich S., 2012, MNRAS, 425, 2817
 Garrison-Kimmel S., Rocha M., Boylan-Kolchin M., Bullock J., Lally J., 2013, ArXiv e-prints
 Governato F., et al., 2007, MNRAS, 374, 1479
 Governato F., Zolotov A., Pontzen A., Christensen C., Oh S. H., Brooks A. M., Quinn T., Shen S., Wadsley J., 2012, MNRAS, 422, 1231
 Haiman Z., Loeb A., 1997, ApJ, 483, 21
 Hinshaw G., et al., 2012, ArXiv e-prints
 Jenkins A., Frenk C. S., White S. D. M., Colberg J. M., Cole S., Evrard A. E., Couchman H. M. P., Yoshida N., 2001, MNRAS, 321, 372
 Kang X., Macciò A. V., Dutton A. A., 2013, ApJ, 767, 22
 Khlopov M. Y., Kouvaris C., 2008, PRD, 78, 065040
 Klypin A., Kravtsov A. V., Valenzuela O., Prada F., 1999, ApJ, 522, 82
 Komatsu E., et al., 2011, ApJS, 192, 18
 Labbe I., et al., 2010, ApJ, 708, L26
 Macciò A. V., Paduroiu S., Anderhalden D., Schneider A., Moore B., 2012, MNRAS, 424, 1105
 Macciò A. V., Stinson G., Brook C. B., Wadsley J., Couchman H. M. P., Shen S., Gibson B. K., Quinn T., 2012, ApJ, 744, L9
 Mashchenko S., Wadsley J., Couchman H. M. P., 2008, Science, 319, 174
 McQuinn M., O’Leary R. M., 2012, ApJ, 760, 3
 Mesinger A., Perna R., Haiman Z., 2005, ApJ, 623, 1
 Moore B., Frenk C. S., Efstathiou G., Saunders W., 1994, MNRAS, 269, 742
 Moore B., Quinn T., Governato F., Stadel J., Lake G., 1999, MNRAS, 310, 1147
 Papastergis E., Martin A. M., Giovanelli R., Haynes M. P., 2011, ApJ, 739, 38
 Postman M., et al., 2012, ApJS, 199, 25
 Shao S., Gao L., Theuns T., Frenk C. S., 2013, MNRAS, 430, 2346
 Sheth R. K., Tormen G., 1999, MNRAS, 308, 119
 Sobacchi E., Mesinger A., 2013, MNRAS
 Springel V., et al., 2008, MNRAS, 391, 1685
 Tegmark M., et al., 2006, PRD, 74, 123507
 Teyssier R., Pontzen A., Dubois Y., Read J. I., 2013, MNRAS, 429, 3068
 Valageas P., 2012, PRD, 86, 123501
 Viel M., Becker G. D., Bolton J. S., Haehnelt M. G., 2013, ArXiv e-prints
 Viel M., et al., 2008, Physical Review Letters, 100, 041304
 Wang J., White S. D. M., 2007, MNRAS, 380, 93
 Zheng W., et al., 2012, Nature, 489, 406

⁷ See <http://www.stsci.edu/hst/campaigns/frontier-fields>